

COMBINING TRANSFER LEARNING AND SEGMENTATION INFORMATION WITH GANS FOR TRAINING DATA INDEPENDENT IMAGE REGISTRATION

Dwarikanath Mahapatra¹ and Zongyuan Ge^{2,3,*}

² Monash eResearch Center, Monash University, Melbourne, Australia

³ AirDoc Research Australia

¹IBM Research Australia, Melbourne, Australia

*zongyuan.ge@monash.edu

ABSTRACT

Registration is an important task in automated medical image analysis. Although deep learning (DL) based image registration methods outperform time-consuming conventional approaches, they are heavily dependent on training data and do not generalize well for new image types. We present a DL-based approach that can register an image pair which is different from the training images. This is achieved by training generative adversarial networks (GANs) in combination with segmentation information and transfer learning. Experiments on chest Xray and brain MR images show that our method gives better registration performance over conventional methods.

Index Terms— Registration, Segmentation, GANs, Xray, MRI, transfer learning.

1. INTRODUCTION

Important medical image analysis tasks such as atlas building, and monitoring pathological changes over multiple patient visits have deformable image registration as an essential step. Iterative gradient descent methods used in conventional registration methods are slow in practice while deep learning (DL) methods can be very fast at test time. Most DL-based methods rely on large datasets for training. Since it is difficult to obtain ground truth data for registration it restricts the method's efficacy on new image types and in real-world scenarios. A network trained to register a pair of chest Xray images does not perform equally well on a pair of brain magnetic resonance (MR) images, or Xray images from other scanners. Although conventional registration methods are time-consuming, their performance is consistent across different image types. Thus DL-based methods have to be retrained for novel images. In this paper we address this challenge by proposing a DL-based method that, once trained on a particular dataset, can be easily used on other image pairs without extensive retraining.

A comprehensive review of conventional medical image registration methods can be found in [1]. Previous approaches

to DL-based image registration involve the use of convolutional stacked autoencoders (CAE) [2], convolutional neural network (CNN) regressors [3, 4, 5], and CNNs with reinforcement learning [6]. These approaches use a conventional model to generate the transformed image from the predicted deformation field which increases computation time and does not fully utilize the generative capabilities of DL methods. CNNs trained on simulated deformations were used in [7] while in [8] a parameterized registration function is learned from training data, and does not require ground truth.

The above methods are limited by the need of spatially corresponding patches or being too dependent on training data. Generative models can overcome some of these limitations by generating the registered image and the deformation field. In previous work [9] we used generative adversarial networks (GANs) for multimodal retinal image registration, and in [10] show the advantages of including segmentation for registration compared to conventional registration. In this paper we build on our previous works and show how segmentation information can be leveraged to design a DL registration method that does not require extensive retraining when used with different datasets. Our primary contribution is in using principles of transfer learning for achieving dataset-independent registration. We show that our method, despite being trained on chest Xray images, achieves high performance levels with test images of brain MRI.

2. METHODS

In our proposed method the generator network, G , takes two input images: 1) reference image (I^{Ref}), and 2) floating image (I^{Flt}) to be registered to I^{Ref} . The outputs of G are: I^{Trans} , the registered image (transformed version of I^{Flt}); 2) $I^{Def-Recv}$ the recovered deformation field and 3) I_{Seg}^{Trans} the segmentation mask of I^{Trans} . Our method has two parts: 1) model training using segmentation information. We call this part segmented augmented registration (SAR); 2) model finetuning for a new test image pair using transfer learning.

2.1. Segmentation Augmented Registration Using GANs

GANs [11] are generative models where the generator G outputs a desired image type while a discriminator D outputs a probability of the generated image matching the training data. The training database has chest Xray images and the corresponding masks of two lungs. To generate training data the floating images are first affinely aligned to the respective reference images. The aligned images are subjected to local elastic deformation using B-splines with the pixel displacements in the range of $\pm[1, 20]$. We denote this deformation field as $I_{Def-App}$, the applied deformation field. The original images are I^{Ref} and the transformed images are I^{Flt} . G 's parameters θ_G are given by,

$$\hat{\theta} = \arg \min_{\theta_G} \frac{1}{N} \sum_{n=1}^N l^{SAR} \left(G_{\theta_G}(I^{Flt}), I^{Ref}, I^{Flt}, I^{Seg} \right), \quad (1)$$

where the loss function l^{SAR} combines content loss (Eqn. 2) and adversarial loss (Eqn. 3), and $G_{\theta_G}(I^{Flt}) = I^{Trans}$. The content loss is given by

$$l_{content}(I^{Trans}, I^{Ref}) = NMI(I^{Ref}, I^{Trans}) + [1 - SSIM(I^{Ref}, I^{Trans})] + VGG(I^{Ref}, I^{Trans}). \quad (2)$$

NMI denotes normalized mutual information between I^{Ref} and I^{Trans} and $SSIM$ denotes structural similarity index metric (SSIM). VGG is the $L2$ distance between two images using all the multiple feature maps obtained from a pre-trained $VGG16$ network [12]. This sums up to $64 \times 2 + 128 \times 2 + 256 \times 2 + 512 \times 3 + 512 \times 3 = 3968$ feature maps and compares information from multiple scales for better robustness. All feature maps are normalized to values between $[0, 1]$.

Figure 1(a) shows the generator network G which employs residual blocks, each block having two convolutional layers with 3×3 filters and 64 feature maps, followed by batch normalization and ReLU activation. G also outputs a deformation field and the segmentation masks of I^{Trans} , I^{Ref} . The segmentation masks are obtained by fusing the weighted normalized output maps of the different convolution layers and applying Otsu's thresholding. The convolution layer outputs highlight the different anatomies of the image and the weights quantify the importance of each map. Figure 2 shows an example image, the obtained fused convolution mask and the segmented mask by Otsu's thresholding (along with a contour of the manual segmentation and the output of UNet segmentation). This shows that our segmentation mask is very similar to UNet's output.

The discriminator D (Figure 1 (b)) has eight convolutional layers with the kernels increasing by a factor of 2 from 64 to 512. Leaky ReLU is used and strided convolutions reduce the image dimension when the number of features is doubled. The resulting 512 feature maps are followed by two dense layers and a final sigmoid activation to obtain a probability map. D evaluates similarity of intensity distribution

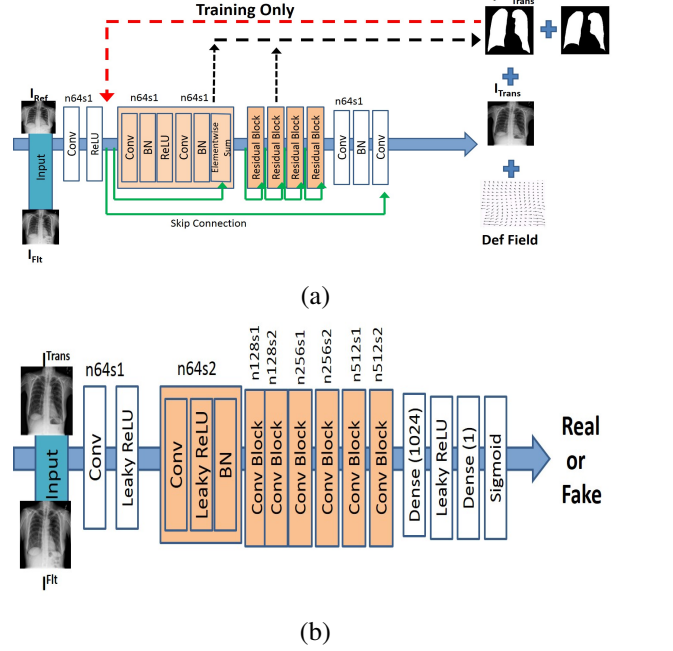


Fig. 1. (a) Generator Network; (b) Discriminator network. $n64s1$ denotes 64 feature maps (n) and stride (s) 1 for each convolutional layer.

between I^{Trans} and I^{Ref} , the accuracy of the two segmentation masks compared to their manual counterparts and the overlap between I_{Seg}^{Trans} and I_{Seg}^{Ref} , and the error between generated and reference deformation fields.

2.2. Adversarial Loss with Segmentation Information

In addition to the content loss (Eqn 2) we have: 1) an adversarial loss; and 2) a cycle consistency loss to ensure transformations G, F do not contradict each other. Since our generator network has multiple outputs we have additional terms for the adversarial loss. The first term matches the distribution of I^{Trans} to I^{Flt} and is given by:

$$L_{cycGAN}(G, D_Y) = E_{y \in p_{data}(y)} [\log D_Y(y)] + E_{x \in p_{data}(x)} [\log (1 - D_Y(G(x)))] , \quad (3)$$

where $X = I^{Flt}$ and $Y = I^{Ref}$. $L_{cycGAN}(F, D_X)$ is the corresponding adversarial loss for F and D_X . The cycle consistency loss [13] ensures the deformation fields are reversible and is achieved by,

$$L_{cyc}(G, F) = E_x \|F(G(x)) - x\|_1 + E_y \|G(F(y)) - y\|_1 , \quad (4)$$

Segmentation information is included in the adversarial loss by calculating the logarithm of the dice metric (DM) between the generated mask I_{Seg}^{Trans} during each training step and I_{Seg}^{Ref} the segmentation mask of I^{Ref} . I_{Seg}^{Trans} is obtained

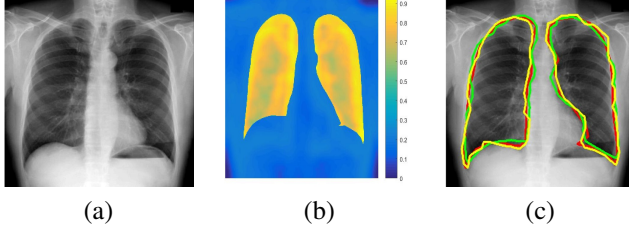


Fig. 2. Example segmentation output from generator network on the fly. (a) original image; (b) fused weighted convolutional map; (c) segmentation outputs - green contour shows mask obtained by Otsu’s thresholding the image in (b), red contour is the manual segmentation, yellow contour is the output of UNet segmentation.

by applying $I^{Def-Recv}$, the recovered deformation field, to I_{Seg}^{Flt} . The third adversarial loss term is the mean square error between $I^{Def-App}$ and $I^{Def-Recv}$, the applied and recovered deformation fields. The final adversarial loss is

$$L_{adv} = L_{cycGAN}(G, D_{I^{Ref}}) + L_{cycGAN}(F, D_{I^{Flt}}) + \log DM(I_{Seg}^{Ref}, I_{Seg}^{Trans}) + \log(1 - MSE_{Norm}(I^{Def-App}, I^{Def-Recv})), \quad (5)$$

where MSE_{Norm} is the MSE normalized to $[0, 1]$, and $1 - MSE_{Norm}$ ensures that similar deformation fields gives a corresponding higher value. All terms in the adversarial loss function have values in $[0, 1]$. The full objective function is

$$L(G, F, D_{I^{Flt}}, D_{I^{Ref}}) = L_{adv} + l_{content} + \lambda L_{cyc}(G, F) \quad (6)$$

where $\lambda = 10$ controls the contribution of the two objectives. The optimal parameters are given by:

$$G^*, F^* = \arg \min_{F, G} \max_{D_{I^{Flt}}, D_{I^{Ref}}} L(G, F, D_{I^{Flt}}, D_{I^{Ref}}) \quad (7)$$

2.3. Registering a new image

The primary advantage of our method is its ability to register a new image pair. During training the trained network G generates the segmentation masks of the input images, the registered image and the deformation field. Since we do not have applied deformation field to determine the accuracy of test image, the best way to gauge registration performance is by comparing I^{Trans} and I^{Ref} based on feature maps and segmentation mask output. If the input test image pair consists of lung images (with training images also of the lung) the generated outputs will be close to the desired values and there is no need for any finetuning of the weights.

The challenge lies in registering a completely new image pair, e.g., brain MR images which we achieve by transfer learning. In transfer learning for image classification the weights of all except the last few layers are frozen. We use a similar principle to register a new test image pair. The weights

of the last convolution layer of generator G are updated iteratively based on the output of the discriminator. In the case of registering a new test image pair, the network is being finetuned. As a result, the discriminator network also comes into play. However, in this case the adversarial loss is based on the cyclic GAN and segmentation mask loss terms, i.e., the first three terms of Eqn. 5, and the deformation field loss term is excluded. The weight updates occur till the difference of cost function values for consecutive iterations is less than 1%. The update happens for 10 – 30 iterations depending on the input image pair. Since the weight updates are only for the last layer and the computation is GPU based, the time taken for registration is very low, around 0.3 – 0.5 seconds.

3. EXPERIMENTS

Our registration method was trained on the NIH ChestXray14 dataset [14]. The original dataset contains 112,120 frontal-view X-rays with 14 disease labels. To make it suitable for registration we selected images from 50 with multiple visits. The first visit image was I^{Ref} and subsequent images were I^{Flt} . In total we selected 906 images where each patient had minimum 3 images and maximum 8 images. The left and right lung were manually outlined in each image. All images were resized to 512×512 pixels before the manual annotations. For all our experiments we split the dataset into training, validation and test sets comprising of 70, 10, 20% of the images. The split was done at the patient level such that images from a single patient were in one fold only. All the reported results are for the test set. Registration performance was validated using mean absolute distance (MAD), the 95% Hausdorff Distance (HD_{95}) and Dice Metric (DM). After training on chest xray images we apply our method to brain and cardiac MR images with finetuning.

Our method was implemented in TensorFlow using Adam [15] with $\beta_1 = 0.93$ and batch normalization. The generator network G was trained with a learning rate of 0.001 and 10^5 update iterations. Mean square error (MSE) based ResNet was used to initialize G . The final GAN was trained with 10^5 update iterations at learning rate 10^{-3} . Training and test was performed on a NVIDIA Tesla K40 GPU with 12 GB RAM.

We show results for: 1) $SARNet$ - our proposed registration network; 2) SAR_{NoSeg} - SAR without using segmentation information; 3) $FlowNet$ - the registration method of [4]; 4) $DIRNet$ - the method of [5]; 5) $Voxel Morph$ - the registration method of [8]; and 6) a conventional registration method Elastix [16]. All networks were trained on lung images and applied to brain images. The average training time for an augmented dataset with 98,000 images is 36 hours. The following parameter settings were used for Elastix: non rigid registration using normalized mutual information (NMI) as the cost function. Nonrigid transformations are modelled by B-splines [17], embedded in a multi-grid setting. The grid spacing was set to 80, 40, 20, 10, 5 mm with the correspond-

	Bef. Reg	After Registration		
		SAR Net	SAR <i>NoSeg</i>	DIR Net
DM(%)	67.2	74.1	71.2	70.9
HD ₉₅ (mm)	14.5	10.8	12.3	12.7
MAD	16.1	12.0	13.6	14.1
Time(s)		0.5	0.4	0.6
	Flow Net	After Registration		
		GC -SAR	Elastix	Voxel Morph
DM(%)	69.4	70.2	70.3	71.3
HD ₉₅ (mm)	14.1	13.8	14.2	13.6
MAD	15.1	15.3	15.9	14.2
Time(s)	0.5	0.6	21	0.5

Table 1. Registration results for brain images when network is trained on lung images.

ing downsampling factors being 4, 3, 2, 1, 1.

3.1. Registration Results For Brain MRI

We use the 800 images of the ADNI-1 dataset [18] consisting of 200 controls, 400 MCI and 200 Alzheimer’s Disease patients. The MRI protocol for ADNI1 focused on consistent longitudinal structural imaging on 1.5T scanners using T1 and dual echo T2-weighted sequences. All scans were resampled to $256 \times 256 \times 256$ with 1mm isotropic voxels. Pre-processing includes affine registration and brain extraction using FreeSurfer [19]. The atlas is an average of multiple volumes and obtained by aligning MR volumes from [19].

We show the reference image (or the atlas image) in Figure 3 (a) followed by an example floating image in Figure 3 (b). The ventricle structure to be aligned is shown in red in both images. Figures 3 (c)-(i) show the deformed structures obtained by applying the registration field obtained from different methods to the floating image and superimposing these structures on the atlas image. The deformed structures from the floating image are shown in green. In case of a perfect registration the green and red contours should coincide.

Table 1 shows the results of brain registration before and after registration. Our method and [8] perform the best, with ours better. The results clearly demonstrate that our method can effectively transfer learned information from one dataset to another. All other methods have been trained on the brain images. Despite that fact our method outperforms them indicating the importance of using segmentation information in better registration. When the training and test images are of different types then the final registration output requires between 10 – 30 iterations but the time is not noticeable since our experiments are done on GPUs.

Baseline Performance Table 2 summarizes performance using brain MRI for training and test. A 5-fold cross validation uses all the 800 images as part of the test set exactly once

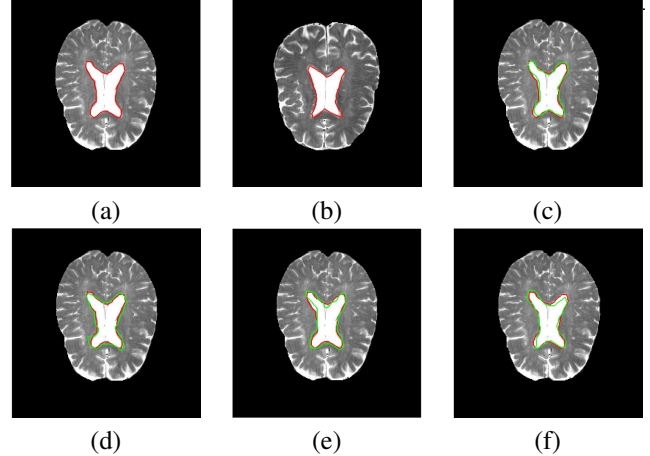


Fig. 3. Results for atlas based brain MRI image registration. (a) I_{Ref} with I_{Ref}^{Seg} (b) I_{Flt} with I_{Flt}^{Seg} . Superimposed registered mask (in green) obtained using: (c) $SAR - Net$; (d)[8]; (e) SAR_{NoSeg} ; and (f) $DIR - Net$.

	Bef. Reg	After Registration		
		SAR Net	SAR <i>NoSeg</i>	DIR Net
DM(%)	67.2	74.9	72.0	71.7
HD ₉₅ (mm)	14.5	10.3	11.9	12.1
MAD	16.1	11.4	13.1	13.7
Time(s)		0.5	0.4	0.6
	Flow Net	After Registration		
		GC -SAR	Elastix	Voxel Morph
DM(%)	70.6	70.9	71.2	72.1
HD ₉₅ (mm)	13.8	13.4	13.5	13.0
MAD	14.6	14.8	15.4	13.8
Time(s)	0.5	0.6	21	0.5

Table 2. Registration results for brain images when network is trained on brain images.

which provides a fair comparison with the numbers in Table 1. Results show that transfer learning gives results similar to when the training and test images are of the same type. This proves the efficacy of our proposed transfer learning based image registration.

4. CONCLUSION

We propose a novel deep learning framework to register brain MR images by training on lung Xray images. We leverage segmentation information and transfer learning with generative adversarial networks. Experimental results show our approach achieves registration with almost similar accuracy as one would obtain when the training and test dataset consist of similar images.

5. REFERENCES

- [1] J.B.A. maintz and M.A. Viergever, "A survey of medical image registration," *Med. Imag. Anal.*, vol. 2, no. 1, pp. 1–36, 1998.
- [2] G. Wu, M. Kim, Q. Wang, B. C. Munsell, , and D. Shen., "Scalable high performance image registration framework by unsupervised deep feature representations learning.," *IEEE Trans. Biomed. Engg.*, vol. 63, no. 7, pp. 1505–1516, 2016.
- [3] S. Miao, Y. Zheng Z.J. Wang, and R. Liao, "Real-time 2d/3d registration via cnn regression," in *IEEE ISBI*, 2016, pp. 1430–1434.
- [4] A. Dosovitskiy, P. Fischer, and et. al., "Flownet: Learning optical flow with convolutional networks," in *In Proc. IEEE ICCV*, 2015, pp. 2758–2766.
- [5] B. de Vos, F. Berendsen, M.A. Viergever, M. Staring, and I. Isgum, "End-to-end unsupervised deformable image registration with a convolutional neural network," in *arXiv preprint arXiv:1704.06065*, 2017.
- [6] R. Liao, S. Miao, P. de Tournemire, S. Grbic, A. Kamen, T. Mansi, and D. Comaniciu, "An artificial agent for robust image registration," in *AAAI*, 2017, pp. 4168–4175.
- [7] H. Sokooti, B. de Vos, F. Berendsen, B.P.F. Lelieveldt, I. Isgum, and M. Staring, "Nonrigid image registration using multiscale 3d convolutional neural networks," in *MICCAI*, 2017, pp. 232–239.
- [8] G. Balakrishnan, A. Zhao, M.R. Sabuncu, and J. Guttag, "An supervised learning model for deformable medical image registration," in *Proc. CVPR*, 2018, pp. 9252–9260.
- [9] D. Mahapatra, B. Antony, S. Sedai, and R. Garnavi, "Deformable medical image registration using generative adversarial networks," in *In Proc. IEEE ISBI*, 2018, pp. 1449–1453.
- [10] D. Mahapatra, Z. Ge, S. Sedai, and R. Chakravorty., "Joint registration and segmentation of xray images using generative adversarial networks," in *In Proc. MICCAI-MLMI*, 2018, pp. 73–80.
- [11] I. Goodfellow, J. Pouget-Abadie, M. Mirza, B. Xu, D. Warde-Farley, S. Ozair, A. Courville, and Y. Bengio, "Generative adversarial nets," in *Proc. NIPS*, 2014, pp. 2672–2680.
- [12] K. Simonyan and A. Zisserman., "Very deep convolutional networks for large-scale image recognition," *CoRR*, vol. abs/1409.1556, 2014.
- [13] J.Y. Zhu, T.park, P. Isola, and A.A. Efros, "Un⁵paired image-to-image translation using cycle-consistent adversarial networks," in *arXiv preprint arXiv:1703.10593*, 2017.
- [14] X. Wang, Y. Peng, L. Lu, Z. Lu, M. Bagheri, and R.M. Summers, "Chestx-ray8: Hospital-scale chest x-ray database and benchmarks on weakly-supervised classification and localization of common thorax diseases," in *In Proc. CVPR*, 2017.
- [15] D.P. Kingma and J. Ba, "Adam: A method for stochastic optimization," in *arXiv preprint arXiv:1412.6980*, 2014.
- [16] S. Klein, M. Staring, K. Murphy, M.A. Viergever, and J.P.W. Pluim., "Elastix: a toolbox for intensity based medical image registration.," *IEEE Trans. Med. Imag.*, vol. 29, no. 1, pp. 196–205, 2010.
- [17] D. Rueckert, L.I. Sonoda, C. Hayes, D.L.G Hill, M.O Leach, and D.J Hawkes., "Nonrigid registration using free-form deformations: application to breast mr images.," *IEEE Trans. Med. Imag.*, vol. 18, no. 8, pp. 712–721, 1999.
- [18] S. G. Mueller, "Ways toward an early diagnosis in alzheimers disease: the alzheimers disease neuroimaging initiative (ADNI).," *Alzheimers & Dementia*, vol. 1, no. 1, pp. 55–66, 2005.
- [19] B. Fischl, "Freesurfer," *Neuroimage*, vol. 62, no. 2, pp. 774–781, 2015.
- [20] D. Mahapatra, "Semi-supervised learning and graph cuts for consensus based medical image segmentation," *Pattern Recognition*, vol. 63, no. 1, pp. 700–709, 2017.
- [21] J. Zilly, J.M. Buhmann, and D. Mahapatra, "Glaucoma detection using entropy sampling and ensemble learning for automatic optic cup and disc segmentation.," *In Press Computerized Medical Imaging and Graphics*, vol. 55, no. 1, pp. 28–41, 2017.
- [22] D. Mahapatra, F.M. Vos, and J.M. Buhmann, "Active learning based segmentation of crohns disease from abdominal mri.," *Computer Methods and Programs in Biomedicine*, vol. 128, no. 1, pp. 75–85, 2016.
- [23] D. Mahapatra and J. Buhmann, "Visual saliency based active learning for prostate mri segmentation.," *SPIE Journal of Medical Imaging*, vol. 3, no. 1, 2016.
- [24] D. Mahapatra, "Combining multiple expert annotations using semi-supervised learning and graph cuts for medical image segmentation.," *Computer Vision and Image Understanding*, vol. 151, no. 1, pp. 114–123, 2016.

- [25] Z. Li, D. Mahapatra, J. Tielbeek, J. Stoker, L. van Vliet, and F.M. Vos, "Image registration based on autocorrelation of local structure.," *IEEE Trans. Med. Imaging*, vol. 35, no. 1, pp. 63–75, 2016.
- [26] D. Mahapatra, "Automatic cardiac segmentation using semantic information from random forests.," *J. Digit. Imaging*, vol. 27, no. 6, pp. 794–804, 2014.
- [27] D. Mahapatra, S. Gilani, and M.K. Saini., "Coherency based spatio-temporal saliency detection for video object segmentation.," *IEEE Journal of Selected Topics in Signal Processing*, vol. 8, no. 3, pp. 454–462, 2014.
- [28] D. Mahapatra and J.M. Buhmann, "Analyzing training information from random forests for improved image segmentation.," *IEEE Trans. Imag. Proc.*, vol. 23, no. 4, pp. 1504–1512, 2014.
- [29] D. Mahapatra and J.M. Buhmann, "Prostate mri segmentation using learned semantic knowledge and graph cuts.," *IEEE Trans. Biomed. Engg.*, vol. 61, no. 3, pp. 756–764, 2014.
- [30] D. Mahapatra, J. Tielbeek, J.C. Makanyanga, J. Stoker, S.A. Taylor, F.M. Vos, and J.M. Buhmann, "Automatic detection and segmentation of crohn's disease tissues from abdominal mri.," *IEEE Trans. Med. Imaging*, vol. 32, no. 12, pp. 1232–1248, 2013.
- [31] D. Mahapatra, J. Tielbeek, F.M. Vos, and J.M. Buhmann, "A supervised learning approach for crohn's disease detection using higher order image statistics and a novel shape asymmetry measure.," *J. Digit. Imaging*, vol. 26, no. 5, pp. 920–931, 2013.
- [32] D. Mahapatra, "Cardiac mri segmentation using mutual context information from left and right ventricle.," *J. Digit. Imaging*, vol. 26, no. 5, pp. 898–908, 2013.
- [33] D. Mahapatra, "Cardiac image segmentation from cine cardiac mri using graph cuts and shape priors.," *J. Digit. Imaging*, vol. 26, no. 4, pp. 721–730, 2013.
- [34] D. Mahapatra, "Joint segmentation and groupwise registration of cardiac perfusion images using temporal information.," *J. Digit. Imaging*, vol. 26, no. 2, pp. 173–182, 2013.
- [35] D. Mahapatra, "Skull stripping of neonatal brain mri: Using prior shape information with graphcuts.," *J. Digit. Imaging*, vol. 25, no. 6, pp. 802–814, 2012.
- [36] D. Mahapatra and Y. Sun, "Integrating segmentation information for improved mrf-based elastic image registration.," *IEEE Trans. Imag. Proc.*, vol. 21, no. 1, pp. 170–183, 2012.
- [37] D. Mahapatra and Y. Sun, "Mrf based intensity invariant elastic registration of cardiac perfusion images using saliency information.," *IEEE Trans. Biomed. Engg.*, vol. 58, no. 4, pp. 991–1000, 2011.
- [38] D. Mahapatra and Y. Sun, "Rigid registration of renal perfusion images using a neurobiology based visual saliency model.," *EURASIP Journal on Image and Video Processing*, pp. 1–16, 2010.
- [39] D. Mahapatra, S. Bozorgtabar, J.-P. Thiran, and M. Reyes, "Efficient active learning for image classification and segmentation using a sample selection and conditional generative adversarial network.," in *In Proc. MICCAI (2)*, 2018, pp. 580–588.
- [40] J. Zilly, J. Buhmann, and D. Mahapatra, "Boosting convolutional filters with entropy sampling for optic cup and disc image segmentation from fundus images.," in *In Proc. MLMI*, 2015, pp. 136–143.
- [41] D. Mahapatra and J. Buhmann, "Visual saliency based active learning for prostate mri segmentation.," in *In Proc. MLMI*, 2015, pp. 9–16.
- [42] D. Mahapatra and J. Buhmann, "Obtaining consensus annotations for retinal image segmentation using random forest and graph cuts.," in *In Proc. OMI*, 2015, pp. 41–48.
- [43] D. Mahapatra and J.M. Buhmann, "A field of experts model for optic cup and disc segmentation from retinal fundus images.," in *In Proc. IEEE ISBI*, 2015, pp. 218–221.
- [44] D. Mahapatra, Z. Li, F.M. Vos, and J.M. Buhmann, "Joint segmentation and groupwise registration of cardiac dce mri using sparse data representations.," in *In Proc. IEEE ISBI*, 2015, pp. 1312–1315.
- [45] D. Mahapatra, F.M. Vos, and J.M. Buhmann, "Crohn's disease segmentation from mri using learned image priors.," in *In Proc. IEEE ISBI*, 2015, pp. 625–628.
- [46] H. Kuang, B. Guthier, M. Saini, D. Mahapatra, and A. El Saddik, "A real-time smart assistant for video surveillance through handheld devices.," in *In Proc: ACM Intl. Conf. Multimedia*, 2014, pp. 917–920.
- [47] D. Mahapatra, J. Tielbeek, J.C. Makanyanga, J. Stoker, S.A. Taylor, F.M. Vos, and J.M. Buhmann, "Combining multiple expert annotations using semi-supervised learning and graph cuts for crohn's disease segmentation.," in *In Proc: MICCAI-ABD*, 2014.
- [48] D. Mahapatra, J. Tielbeek, J.C. Makanyanga, J. Stoker, S.A. Taylor, F.M. Vos, and J.M. Buhmann, "Active learning based segmentation of crohn's disease using

- principles of visual saliency,” in *Proc. IEEE ISBI*, 2014, pp. 226–229.
- [49] D. Mahapatra, P. Schüffler, J. Tielbeek, F.M. Vos, and J.M. Buhmann, “Semi-supervised and active learning for automatic segmentation of crohn’s disease,” in *Proc. MICCAI, Part 2*, 2013, pp. 214–221.
- [50] D. Mahapatra, “Graph cut based automatic prostate segmentation using learned semantic information,” in *Proc. IEEE ISBI*, 2013, pp. 1304–1307.
- [51] D. Mahapatra and J.M. Buhmann, “Automatic cardiac rv segmentation using semantic information with graph cuts,” in *Proc. IEEE ISBI*, 2013, pp. 1094–1097.
- [52] D. Mahapatra, J. Tielbeek, F.M. Vos, and J.M. Buhmann, “Weakly supervised semantic segmentation of crohn’s disease tissues from abdominal mri,” in *Proc. IEEE ISBI*, 2013, pp. 832–835.
- [53] D. Mahapatra, J. Tielbeek, F.M. Vos, and J.M. Buhmann, “Crohn’s disease tissue segmentation from abdominal mri using semantic information and graph cuts,” in *Proc. IEEE ISBI*, 2013, pp. 358–361.
- [54] D. Mahapatra, J. Tielbeek, F.M. Vos, and J.M. Buhmann, “Localizing and segmenting crohn’s disease affected regions in abdominal mri using novel context features,” in *Proc. SPIE Medical Imaging*, 2013.
- [55] D. Mahapatra, J. Tielbeek, J.M. Buhmann, and F.M. Vos, “A supervised learning based approach to detect crohn’s disease in abdominal mr volumes,” in *Proc. MICCAI workshop Computational and Clinical Applications in Abdominal Imaging(MICCAI-ABD)*, 2012, pp. 97–106.
- [56] D. Mahapatra, “Cardiac lv and rv segmentation using mutual context information,” in *Proc. MICCAI-MLMI*, 2012, pp. 201–209.
- [57] D. Mahapatra, “Landmark detection in cardiac mri using learned local image statistics,” in *Proc. MICCAI-Statistical Atlases and Computational Models of the Heart. Imaging and Modelling Challenges (STACOM)*, 2012, pp. 115–124.
- [58] F. M. Vos, J. Tielbeek, R. Naziroglu, Z. Li, P. Schüffler, D. Mahapatra, Alexander Wiebel, C. Lavini, J. Buhmann, H. Hege, J. Stoker, and L. van Vliet, “Computational modeling for assessment of IBD: to be or not to be?,” in *Proc. IEEE EMBC*, 2012, pp. 3974–3977.
- [59] D. Mahapatra, “Groupwise registration of dynamic cardiac perfusion images using temporal information and segmentation information,” in *In Proc: SPIE Medical Imaging*, 2012.
- [60] D. Mahapatra, “Neonatal brain mri skull stripping using graph cuts and shape priors,” in *In Proc: MICCAI workshop on Image Analysis of Human Brain Development (IAHBD)*, 2011.
- [61] D. Mahapatra and Y. Sun, “Orientation histograms as shape priors for left ventricle segmentation using graph cuts,” in *In Proc: MICCAI*, 2011, pp. 420–427.
- [62] D. Mahapatra and Y. Sun, “Joint registration and segmentation of dynamic cardiac perfusion images using mrfs.,” in *Proc. MICCAI*, 2010, pp. 493–501.
- [63] D. Mahapatra and Y. Sun., “An mrf framework for joint registration and segmentation of natural and perfusion images,” in *Proc. IEEE ICIP*, 2010, pp. 1709–1712.
- [64] D. Mahapatra and Y. Sun, “Retrieval of perfusion images using cosegmentation and shape context information,” in *Proc. APSIPA Annual Summit and Conference (ASC)*, 2010.
- [65] D. Mahapatra and Y. Sun, “A saliency based mrf method for the joint registration and segmentation of dynamic renal mr images,” in *Proc. ICDIP*, 2010.
- [66] D. Mahapatra and Y. Sun, “Nonrigid registration of dynamic renal MR images using a saliency based MRF model,” in *Proc. MICCAI*, 2008, pp. 771–779.
- [67] D. Mahapatra and Y. Sun, “Registration of dynamic renal mr images using neurobiological model of saliency,” in *Proc. ISBI*, 2008, pp. 1119–1122.
- [68] D. Mahapatra, M.K. Saini, and Y. Sun, “Illumination invariant tracking in office environments using neurobiology-saliency based particle filter,” in *IEEE ICME*, 2008, pp. 953–956.
- [69] D. Mahapatra, S. Roy, and Y. Sun, “Retrieval of mr kidney images by incorporating spatial information in histogram of low level features,” in *In 13th International Conference on Biomedical Engineering*, 2008.
- [70] D. Mahapatra and Y. Sun, “Using saliency features for graphcut segmentation of perfusion kidney images,” in *In 13th International Conference on Biomedical Engineering*, 2008.
- [71] D. Mahapatra, S. Winkler, and S.C. Yen, “Motion saliency outweighs other low-level features while watching videos,” in *SPIE HVEL.*, 2008, pp. 1–10.
- [72] D. Mahapatra, A. Routray, and C. Mishra, “An active snake model for classification of extreme emotions,” in *IEEE International Conference on Industrial Technology (ICIT)*, 2006, pp. 2195–2199.